Journal of Materials Chemistry B

ROYAL SOCIETY OF CHEMISTRY

PAPER

View Article Online
View Journal | View Issue

Check for updates

Cite this: J. Mater. Chem. B, 2021, 9, 9153

LSPR immuno-sensing based on iso-Y nanopillars for highly sensitive and specific imidacloprid detection†

Ambra Vestri, ‡*[a] Massimo Rippa, ‡[a] Valentina Marchesano,[a] Domenico Sagnelli,[a] Giancarlo Margheri,[b] Jun Zhou [c] and Lucia Petti *[a]

Received 23rd June 2021,
Accepted 3rd October 2021

DOI: 10.1039/d1tb01344k

rsc.li/materials-b

Imidacloprid is the most widely used insecticide in agriculture and its intensive use over the last 30 years has caused a global concern due to its potentially toxic effects on the ecosystem. Considering the recent scientific interest in novel simple methods for imidacloprid analysis, we propose a label-free sensitive and specific localised surface plasmon resonance system for the detection of the insecticide based on 2D nanostructured metasurfaces with highly performing plasmonic properties. The specificity of the sensor proposed was achieved by covalent bio-functionalization of the metasurface using a smart and easy one-step procedure mediated by carbon disulphide. The biosensor produced was tested using a set of imidacloprid standard solutions showing a competitive limit of detection, lower than 1 ng mL^{-1}. Our novel nanosensing configuration represents a valid and reliable solution to realize low-cost portable POC tests as an alternative to the laborious and expensive methods traditionally used for insecticide detection.

1. Introduction

Imidacloprid is a systemic insecticide belonging to the family of the neonicotinoid compounds. The name of this class of insecticides means "new nicotine-like insecticides" and it arises from the chemical structure resemblance between these compounds and nicotine.[1,2] The presence of the nitroimine group in imidacloprid allows the insecticide to exhibit selective lethal effects against their invertebrate target, acting as agonists on the postsynaptic nicotinic acetylcholine receptors (nAChRs).[3] In particular, the ligand-gated ion channel nAChRs are irreversibly bound by the insecticide with a consequent overstimulation of cholinergic synapses finally resulting in the paralysis and death of the insect.[1] Despite the low toxicity of imidacloprid in mammals[4] chronic exposure to sublethal doses still seems to pose risks in these species, humans included.[5,6] Moreover, the widespread and intensive use of imidacloprid over the last 30 years for many agricultural and residential purposes has provoked a rising global concern because of the imidacloprid non-target effects on living beings important for the ecosystem, such as aquatic organisms and pollinators.[7–11] The gold standard methods in use for imidacloprid detection, such as liquid chromatography–tandem mass spectrometry, have excellent performance but are complex, expensive and not suitable for on-site analysis. The design of novel, simple and cost effective analytical methods for imidacloprid has been in high demand in recent scientific literature.[12] A SPR system coupled with a smartphone for the qualitative/semiquantitative detection of imidacloprid was proposed in 2016 by the Pei-Kuen Wei group.[13] The chip was fabricated on a polymeric substrate using a complex procedure that involved hot embossing nanoimprint lithography in order to realize capped silver nanoslits encapsulated by an Al_2O_3 film. Although the system allowed a visual detection limit (DL) of $\approx$1 ppb and a working concentration range of 1 ppb–10 ppm, the system was characterized by limited resolution and poor sensitivity. A renewed system with an improved spectral resolution $\approx$0.1 nm per pixel, a DL $\approx$ 10 ppb and a detection time $\approx$ 2 h 30 min has been recently proposed by the same authors.[14] A quench-body immunoassay for imidacloprid detection was then proposed in 2018 by Zhao *et al.*[15] It was realized by means of a recombinant antibody antigen-binding fragment carrying a Cys-tag for fluorescence labelling. This strategy involved a dye coupling reaction, expensive reagents, and different steps of purification after expression. The immunoassay was characterized by low cross-reactivity (1.7–3.2%) and a LOD of 10 ng mL^{-1} (= 10 ppb). Electrochemistry was also exploited to realize an imidacloprid sensor. El-Akaad *et al.* has recently reported a

[a] Institute of Applied Sciences and Intelligent Systems "E. Caianiello" of CNR, Pozzuoli 80072, Italy. E-mail: ambra.vestri@isasi.cnr.it, lucia.petti@cnr.it
[b] Institute for Complex Systems of CNR, Sesto Fiorentino 50019, Italy
[c] Institute of Photonics, Faculty of Science, Ningbo University, Ningbo, People's Republic of China

† Electronic supplementary information (ESI) available. See DOI: 10.1039/d1tb01344k
‡ These authors contributed equally to this work.

reusable capacitive sensor based on a molecularly imprinted polymer (MIP) (particle size < 1 μm) for insecticide detection with a limit of detection (LOD) of 4.61 μM.[16] Zhang *et al.* used MIP as a recognition element to realize an electrochemical sensor based on a ratiometric strategy found a LOD = 47 nM (12 ng mL^{-1}).[17] Among the variety of transduction elements that can be adopted for the simple, label-free, cost-effective and on-site investigation of hazardous agents to ensure environmental protection and food safety, localized surface plasmon resonance (LSPR) has proved to be particularly favourable.[18] This phenomenon exploits a coherent oscillation of the conduction electrons generated in metallic nanoelements upon interaction with photons of appropriate wavelength, causing both transmitted light attenuation and electric near-field amplification. Refractive index (RI) variations due to the deposition of molecules on the metallic surface can be simply and promptly revealed by evaluating the red shift of the wavelength associated with the transmitted light minimum, allowing a quantitative label-free analysis.[19–22] Compared with other plasmonic approaches, LSPR sensing does not require temperature control or complicated coupling optical systems and, moreover, it allows the design of cheap portable prototype devices (costs less than $5000).[23] The most sensitive region to RI changes is in close proximity to the metal surface; indeed the electromagnetic field quickly decreases over a 10–15 nm distance from the plasmonic area.[24,25] LSPR sensors are commonly realized by exploiting nanoparticles in solution or nanostructured metal surfaces (on a solid support) realized by top-down approaches or bottom-up assembly, and they can be made using different metals and in a plethora of shapes and sizes.[19–21,26–30] Nanopatterned-surfaces, in particular, show different performances according to their pattern features such as geometry, symmetry, element sizes and inter-particle distances. Photonic crystals based on iso-Y-shaped-nanopillars (NPs) have shown interesting plasmonic properties.[31,32] In this work we exploit a 2D periodic arrangement of iso-Y gold NPs to realize an engineered chip for the imidacloprid detection by LSPR. We designed and fabricated the pattern using the Electron Beam Lithography (EBL) technique. Its plasmonic features were explored both numerically, using FEM simulations, and experimentally, analysing the spectral properties and measuring its bulk sensitivity.[33] The nanopatterned surface was functionalized using a monoclonal antibody (Ab) to confer specificity on the proposed biosensor. An easy smart one-step method mediated by carbon disulphide (CS_2) was adopted for the Ab covalent immobilization. Using our biofunctionalized nanostructures as LSPR sensors, we demonstrate the possibility of detecting small amounts (<1 ng mL^{-1}) of the investigated insecticide. We carry out our analysis performing measurements of the LSPR shift in the presence of different concentrations of imidacloprid and realizing comparative tests with other pesticides to evaluate the specificity of our system. Our results suggest that this device is promising for the development of a simple, rapid, sensitive and specific sensor for detection of imidacloprid in water. It can be a valid alternative to traditional methods and, in addition, can be integrated using other chemical on-chip devices to realize compact and cost-effective portable point-of-care (POC) systems.

2. Experimental

2.1 2D nanostructure fabrication

An EBL system (Raith150) was used to fabricate a two-dimensional array with size 200 × 200 μm based on a unit cell arranged in a periodic configuration. The unit cell consists of gold NPs with iso-Y shape and with the size of the branches S1 = 100 nm and S2 = 60 nm (inset of Fig. 1a). The cells are arranged in a triangular lattice with side of $600/\sqrt{3}$ nm. The nanostructured substrate was fabricated making use of conventional EBL fabrication steps. A film of 150 nm thickness of the positive resist styrene methyl acrylate, co-polymer (ZEP520A) was spin coated onto a BK7 glass substrate coated with 15 nm of indium tin oxide (ITO). The substrate was baked at 170° for 5 min and successively exposed to the 22 pA electron beam current with an area dose of 24 μC cm^{-2} to generate a pattern based on the iso-Y shaped nanoholes in the photoresist film. Layer development was achieved by immersing the sample in *n*-amyl acetate (90 s), in a 1 : 3 solution of MIBK: isopropyl alcohol (IPA) (60 s) and, finally in IPA for 30 s. Subsequently, 2 nm Cr and 50 nm Au films were evaporated on the sample surface by the means of the SISTEC CL-400C e-beam system. Au lift-off was accomplished by immersing the sample in acetone for 20 min, then in *N*-methyl-pyrrolidinone (NMP) at 80 °C for 5 min and, finally, spraying it with NMP. After these steps, the plasmonic crystal with Au iso-Y NPs arranged with the geometry described above was achieved.

2.2 Morphological and spectroscopic characterization

The plasmonic nanostructure realized was characterized morphologically making use of both scanning electron microscopy (SEM, Raith 150) and atomic force microscopy (AFM, NT-MDT NTEGRA Spectra) in a contactless configuration.

LSPR of the nanostructure was measured and analyzed realizing a spectroscopic characterization based on the extinction signal evaluation. In the set-up, unpolarized white light of a halogen lamp is focused on the nanostructured pattern making use of a 10× (N.A. 0.25) objective that allows a circular light spot of about 400 μm. The transmission signal T *versus* the wavelength λ achieved from the nanostructure was collected using a fiber with a core of 50 μm positioned behind the nanostructure (in proximity to it) and connected to a spectrophotometer (Ocean Optics USB4000, optical resolution ~1 nm). $T\%(\lambda)$ was determined using the relation $T\%(\lambda) = (T(\lambda) - T_d)/(T_{ref}(\lambda) - T_d) \times 100$, where $T_{ref}(\lambda)$ represents the reference transmission spectrum measured out of the nanostructure and T_d represents the dark transmission spectrum achieved by turning off the lamp. Extinction spectra E_s were calculated by the relation $E_s(\lambda) = 100 - T\%(\lambda)$. Mean E_s was calculated from repeated measurements achieved by moving the collection fiber on different areas of the nanostructures.

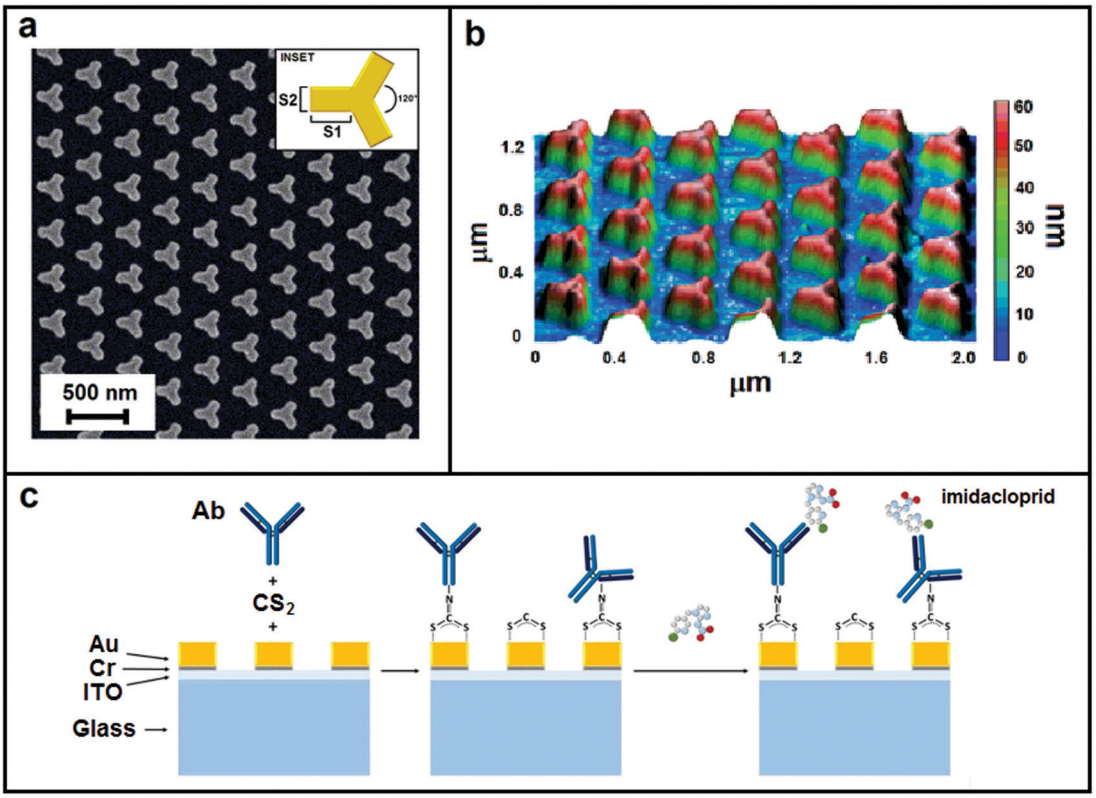

Fig. 1 Nanostructure morphology: (a) SEM image, (b) AFM image and (c) sketch of multilayer and representation of the functionalization steps.

By the mean E_s both the LSPR characteristic of the considered plasmonic nanopattern and its shifts obtained under the different experimental conditions taken into account can be estimated.

In order to evaluate the bulk refractive index sensitivity m of our nanostructure we measured the LSPR peak obtained for five different bulk media: water (n = 1.332), IPA/water 1 : 10 wt/wt (n = 1.341), IPA/water 1 : 5 wt/wt (n = 1.349), IPA/water 1 : 1 wt/wt (n = 1.364), and IPA (n = 1.374) (Fig. 3). The refractive index of the medium was measured making use of an Abbe refractometer.

Using the same setup, we evaluated the spectral shifts $\Delta\lambda_{shift}$ of the LSPR peak achieved for different concentrations of imidacloprid (in PBS solutions) using substrates functionalized as described in the next section. For each concentration taken into account the $\Delta\lambda_{\text{shift}}$ was evaluated as the mean value of 6 measurements realized under the same experimental conditions. The corresponding errors were calculated from the measurements according to the standard deviation relation.

2.3 Nanosensor functionalization and imidacloprid deposition

The biosensor realization was achieved exploiting a one-step functionalization mediated by carbon disulphide to immobilize covalently an anti-imidacloprid monoclonal antibody (CABT-L091S, Creative Diagnostics, NY, USA) on the nanopatterned gold surface. A solution 30 µM CS_2 and 10 µg mL^{-1} anti-imidacloprid monoclonal antibody in PBS was deposited onto the metastructures for 2 h at 4 °C. The biofunctionalized chip was then copiously washed with milliQ water and stored in PBS pH 7.4 a 4 °C until use (by up to 24 h). The biosensor performances were tested using a stock solution 250 µg mL^{-1} imidacloprid (Sigma-Aldrich, Milan, Italy) in milliQ water that was properly diluted in PBS before use. The imidacloprid solution was dropped on the functionalized nanostructures and left to incubate in a humid chamber for 1 h at 25 °C.

After incubation of the analyte, the biosensor was washed 5 times with 1 mL PBS pH 7.4 and dried with N_2 before LSPR spectrum data collection.

2.4 Specificity tests

The biosensor specificity was tested using different no-target pesticides. In particular we used 250 µg mL^{-1} glyphosate in milliQ water and 250 µg mL^{-1} fipronil (TCI-Europe, Zwijndrecht, Belgium) in 50% aqueous ethanol solution as stock solutions. Each pesticide stock solution was diluted down to 400 ng mL^{-1} in PBS pH 7.4 before its deposition on the biosensor surface. After 1 h of incubation in a humid chamber at 25 °C, the biosensor was washed 5 times with 1 mL PBS pH 7.4 and dried with N_2 before LSPR spectrum registration.

In order to reduce the aspecific signal we also adopted a blocking strategy before pesticide deposition onto the biofunctionalized nanostructures. In particular, we used 3% w/w BSA to passivate the sensor surface (1 h at 25 °C, in a humid chamber). The chip was then copiously washed with milliQ water and stored in PBS pH 7.4 at 4 °C until the no-target pesticide deposition.

2.5 Non-specific adsorption test

We prepared a chip biofunctionalized with an anti-glyphosate polyclonal antibody (AS13 2739, Agrisera, Vännäs, Sweden) to verify the lack of imidacloprid non-specific adsorption onto the sensor surface. A solution 30 μM CS_2 and 10 μg mL^{-1} anti-glyphosate monoclonal antibody in PBS was deposited onto the metastructures for 2 h at 4 °C. The biofunctionalized chip was then copiously washed with milliQ water and stored in PBS pH 7.4 a 4 °C until use.

The 250 μg mL^{-1} imidacloprid stock solution was diluted down to 400 ng mL^{-1} in PBS pH 7.4, dropped on the nanostructures and left to incubate in a humid chamber for 1 h at 25 °C.

After analyte incubation, the biosensor was washed 5 times with 1 mL PBS pH 7.4 and dried with N_2 before LSPR spectrum registration.

2.6 Finite element method (FEM) simulation

We performed a three-dimensional numerical simulation using the finite element method FEM (COMSOL Multiphysics® 5.5, Stockholm (Sweden)) to investigate the electric near-field of the plasmonic substrates taken into account. We reproduced the multilayer shown in Fig. 1c considering semi-infinite glass substrate (BK7), semi-infinite air cover, and a thickness for ITO and gold nanopillars respectively of 10 nm and 55 nm. Dispersion relations based on real refractive indices were used for the air, BK7 and ITO while a complex index was considered for gold. At first, we calculated the field on the plane of a singular iso-Y NP (size reported in Section 2.1) when an incident monochromatic source affects it. We performed a parametric sweep calculation for sources with wavelengths ranging between 550 and 1150 nm (step size of 5 nm) and for both x and y polarization. Subsequently, in order to analyze the effects of NP interactions, the field relative to a portion of the considered nanopattern is calculated for an incident source with wavelength of 850 nm and, as in the previous case, with both x and y polarization.

Both types of calculations were performed considering perfectly matched layer (PML) boundary conditions in the z-direction perpendicular to the layers. Furthermore, in the case of an extended pattern, the periodic conditions in both x and y directions were considered. The multilayer was discretized using a tetrahedral mesh with element size in the range 0.5–20 nm. The simulations were performed using a computer with a processor intel core i7, 8 core, 3.40GHz and 32 Gb of RAM.

3. Results and discussion

The nanopattern we consider in this work comprises a periodic arrangement on the triangular base of a unit cell (inset Fig. 1a) made of iso-Y-shaped gold NPs.

We fabricated the nanostructure using the EBL method. As is well known, EBL allows realizing of nano-geometries with high resolution and repeatability but on the other hand it is an expensive and complex technique. Anyway, it is useful to underline that the nanostructures developed using this approach are replicable by other fabrication techniques based on molding or printing, giving the possibility of realizing engineered low-cost devices. In Fig. 1, it is reported the morphological analysis of the nanopattern realized. SEM images in Fig. 1a show how both sizes of the iso-Y NPs and their distance are regular on the whole nanopattern and consistent with the design parameters. The AFM image in Fig. 1b allows estimation of a mean NP height of 54 ± 2 nm. The shape, size and pitch of the NPs determine the main plasmonic characteristics of the structure. Our purpose was to realize a sensing device based on LSPR properties that worked in the near infrared region between 800 nm and 1000 nm. As is well known in the literature, the LSPR-based sensing shows a higher sensitivity in the infrared region than in the visible one.[34–36] Furthermore, a sensor that works in a wavelength range below 1000 nm allows the design of compact devices with lower cost.

The characteristic size of the branches that we chose for the iso-Y cell under consideration (S1 = 100 nm, S2 = 60 nm, see inset Fig. 1a) determines a localized resonance with a peak in air just around 850 nm, allowing a sensing in the spectral region of our interest.

We investigated our nanopattern plasmonic behavior by the means of numerical simulations based on FEM analysis. At first, we investigated the spectral plasmonic field properties of a singular iso-Y NP. We calculated the electric near-field module distributions for both x and y polarized incident monochromatic light for wavelengths in the Vis-NIR range between 550 and 1150 nm and with a wavelength step size of 5 nm. The videos realized with the distributions calculated for both incident polarizations are available in the ESI.† In Fig. 2a we report some frames extrapolated from the animations relative to the fields achieved for the incident wavelengths 550, 700, 850, 1000 and 1150 nm for both x (first line) and y (second line) polarizations. In the figure, the electric fields are normalized regarding the maximum value found. Concerning the shape of the cell considered (Y-shaped), the aim was to increase the density of hot spots shown by the pattern. As known from the literature, the formation of hot spots is favored in proximity of tips and the Y shape taken into account shows a number of tips which is double those shown in the more conventional triangular shape.[36–38] As expected, depending on the polarization used for the FEM analysis, the iso-Y NP shows six hot spots corresponding to the vertices of the different branches that can be associated with the LSPR effects. For both polarizations, the maximum size and intensity of the hot spots are achieved for wavelengths of around 850 nm. In this range the superposition of the two hot spots corresponding to vertices of the same branch is visible and three big hot spots are generated. In order to analyze the effects of NP interactions, we calculated the field relative to an extended portion of the nanopattern. In this case, we consider for calculations a source with a wavelength of 850 nm for which the simulations relative to the singular pillar show high hot spot intensity. Fig. 2b shows the near-field distributions obtained for the x and y polarization. As visible from these last calculations, the plasmonic

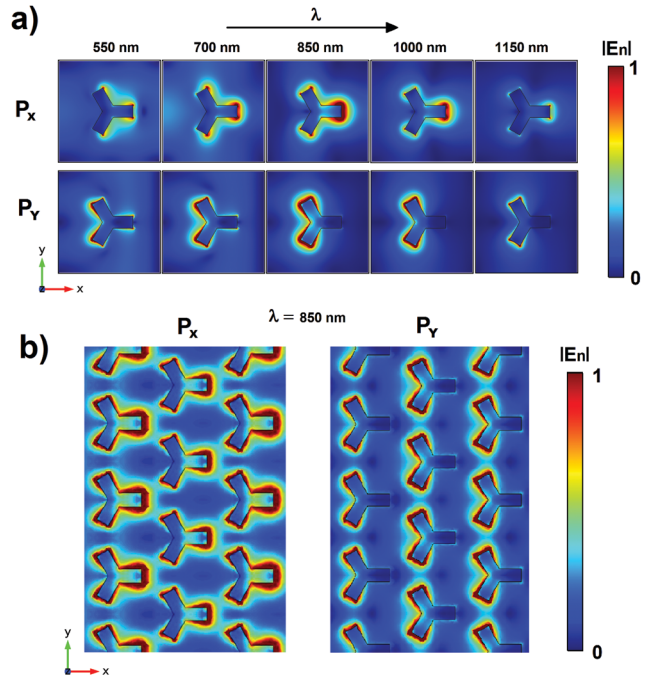

Fig. 2 FEM simulations. Distributions of the normalized module of the electric near-field calculated for both *x* and *y* polarization of the incident source: (a) near-field distributions of a singular iso-Y NPs achieved for different wavelengths of the source, (b) near-field distributions of an extended portion of the nanopattern considered to be achieved for a wavelength of 850 nm.

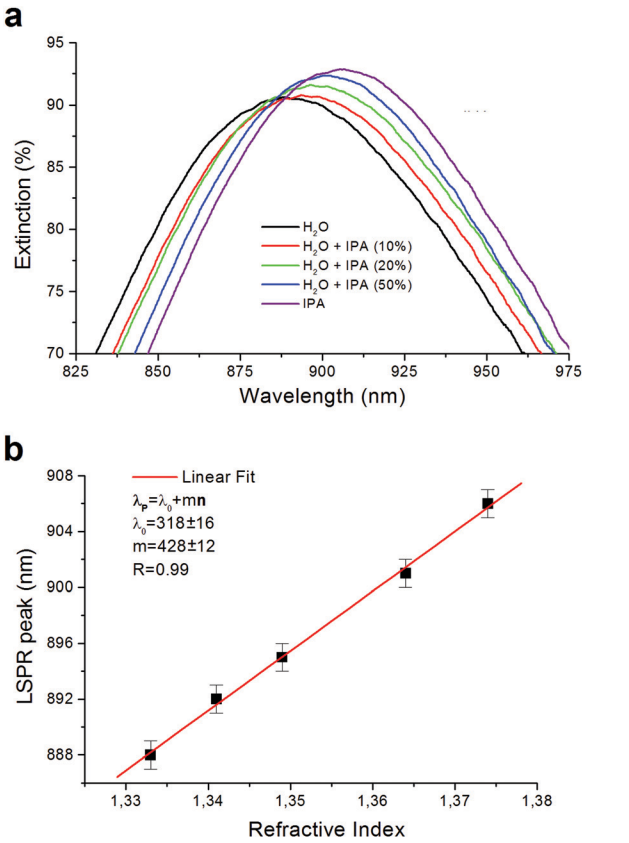

Fig. 3 Spectral characterization of the iso-Y nanopattern: (a) medium extinction spectra measured for different media, (b) linear fit of the LSPR peak wavelength plotted *versus* the refractive index of the medium. The fitting equation is $\lambda_p = 318 + 428 \times n$, with a correlation coefficient $R = 0.99$.

fields of the single NPs interact with each other modifying the distribution and increasing the intensity of the near-field in the regions between the NP branches (dipolar coupling), in particular in the case of an *x* polarized source. It is worth noticing that this interaction could certainly be increased by reducing the distances between the NPs in the geometry considered and, hence, achieving hot spot area with higher intensity. However, this would lead to an increase in the gold filling factor with a consequent reduction in the signal-to-noise ratio relative to the transmission measurements on which our sensing approach is based. For this reason, we believe that the characteristic size taken into account for our nanopattern represents a good compromise to meet these two aspects.

We experimentally evaluated the bulk sensitivity m of the plasmonic nanostructure realized. In Fig. 3a the graph relative to the mean extinction spectra E_s measured for different media as described in Section 2.2 is reported. The LSPR peaks evaluated in the refractive index range 1.332–1.374 are located in the near infrared region (NIR), around 900 nm, and, as expected, they show a red-shift for medium with a higher refractive index. In Fig. 3b, LSPR peaks wavelengths (λ_{peak}) are plotted as a function of the refractive index (n) of the medium showing a good linear trend. For the electromagnetic field with negligible decay length with respect to the effective adsorbate layer thickness, the bulk sensitivity can be estimated using the equation[39] $\lambda_{peak} = \lambda_0 + mn$, where λ_0 is the *y*-intercept and m the bulk sensitivity. Our data are well fitted using the following values: $\lambda_0 = 318 \pm 16$ nm and $m = 428 \pm 12$ nm RIU^{-1}. The sensitivity m that we achieved of 428 nm RIU^{-1} is more than double the average value of about 200 nm RIU^{-1} normally found for 2D nanostructures based on gold nanopillars.[40] The small error bars of 2–3 nm shown in Fig. 3b highlight a high reproducibility of the signal when we move the collecting fiber on the plasmonic pattern. The values of figure-of-merit (FOM) defined as the ratio FOM = m/FWHM (with FWHM being the full wave at half maximum) calculated for the different spectra achieved is about 1.90.

Subsequently, we functionalized the nanopattern to test its performance as the LSPR sensor for specific detection of the imidacloprid. We adopted an easy one-step functionalization strategy for the Ab covalent immobilization mediated by carbon disulphide (CS_2) described in Section 2.3 and represented schematically in Fig. 1c. The CS_2 allows the *in situ* formation of dithiocarbamates (DTCs) exploiting the presence of immunoglobulin G (IgG) amino groups. This strategy was successfully reported in the literature for the bio-functionalization of gold surfaces with proteins, oligonucleotides, amino acids, and small organic molecules.[41–46] DTC chemistry allowed us to achieve a robust gold surface functionalization without introducing linkers taking up the limited LSPR sensing

zone. To the best of our knowledge, this is the first time that this method has been employed for the direct immobilization of antibodies to the sensor surface.

A useful parameter to establish the potential for antigen sensing is to check the amount of antibodies that are immobilized onto the surface, usually expressed in ng mm^{-2} of deposited mass.

This parameter can be evaluated from the measurement of the wavelength shift before and after functionalization with an anti-imidacloprid detecting unit. In fact, when a molecule is adsorbed onto a plasmonic support, the absorption spectrum (angular or spectral) changes, thanks to the surface refractive index variation. If the change Δn is detected in a thin layer whose effective thickness is h, Δn is related to h *via* the relationship proposed by Homola:[47]

$$\Delta n = (\mathrm{d}n/\mathrm{d}c)\Gamma/h$$

where Γ is the surface mass density of the adsorbed layer, $\mathrm{d}n/\mathrm{d}c$ is the variation of refractive index with the concentration of the adsorbed species. As the sensor sensitivity has been evaluated in 428 nm RIU^{-1}, the spectral change of 22 ± 2 nm (immobilization shift) corresponds to a surface refractive index change Δn = 0.051. The value of $\mathrm{d}n/\mathrm{d}c$ is typically 0.1–0.3 mL g^{-1},[47] while the penetration in the external medium of the resonant field, that represents the thickness h of the sensing region, has been estimated to be approximately 10 nm. Taking a typical value of $\mathrm{d}n/\mathrm{d}c$ = 0.2 mg L^{-1}, the corresponding surface mass coverage is readily found to be Γ = 2.5 ng mm^{-2}. As, to our knowledge, the mass coverage of the anti-imidacloprid is a missing value not known in the current literature; however the found value can be compared with figures obtained for its isotype, namely the IgG, linked to the gold surface with chemistries other than CS_2. For instance, in a recent work[48] where α-lipoic acid activated with EDC-NHS chemistry is taken as an IgG immobilizer, a coverage of 24.4 ng mm^{-2} is reported, while a gold linked mixture of mercaptoundecanoic acid (MUA) and propionic acid with EDC-NHS activation led to a gold coverage of 1.2 ng mm^{-2}.[49] A value of 3.4 ng mm^{-2}, has been found for the IgG mass coverage onto an SPR gold chip functionalized with activated MUA,[50] while a lower coverage of 1.5 ng mm^{-2} has been found for IgG coated gold nanoparticles *via* direct immobilization of the antibody.[51] In conclusion, the efficiency of our immobilizing strategy on gold with carbon disulfide is nicely comparable with other ones currently available.

We evaluated the limit of detection (LOD) of our system using equal copies of our bio-functionalized nanostructure. We performed repeated measures of solutions of imidacloprid with the concentration ranging between 0.1 and 2500 ng mL^{-1}. For each measurement, the nanosensor was incubated with a solution of imidacloprid in PBS (pH 7.4), and the LSPR peak measured after washes. The mean LSPR peak shifts ($\Delta\lambda_{shift}$) evaluated are shown in Fig. 4a (black squares). Experimentally, the $\Delta\lambda_{shift}$ grows to a value of about 35 nm corresponding to an imidacloprid concentration of $[I]$ = 1000 ng mL^{-1}, after which the signal reaches a plateau due to the saturation of the

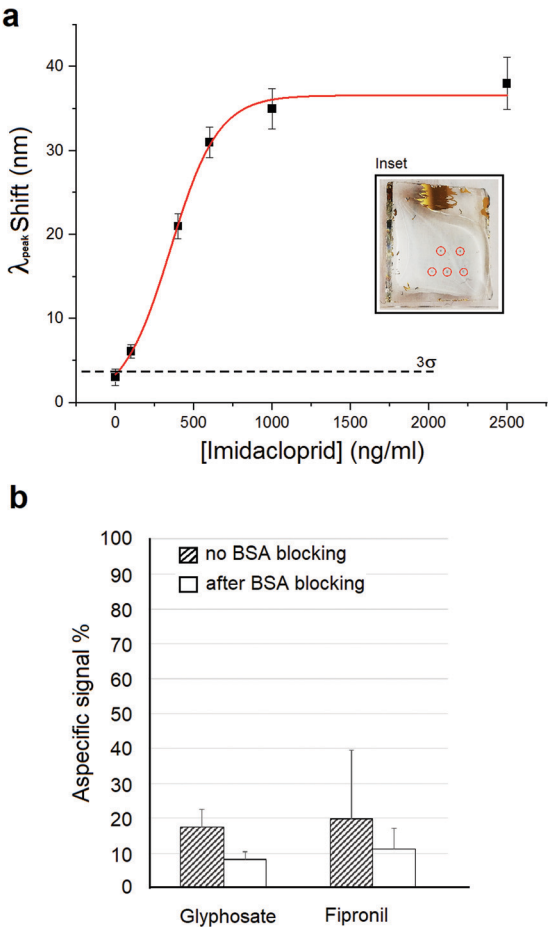

Fig. 4 LSPR sensing of imidacloprid with functionalized iso-Y nanopattern: (a) LOD evaluation for specific imidacloprid detection: λ_{peak} shift *versus* imidacloprid concentration (in the inset, an image of a substrate with some iso-Y nanostructure replicas circled in red), (b) specificity analysis of the functionalized nanopattern carried out considering two other pesticides, glyphosate and fipronil.

nanostructured sensitive area of the sample. We are aware that the imidacloprid $\Delta\lambda_{shift}$ magnitude is particularly high, considering the low molecular weight of this molecule (255 g mol^{-1}). A possible explanation could be the formation of π-stacking interactions among the imidacloprid molecules captured by the antibody and the molecules dispersed in solution, due to the presence of the analyte aromatic ring. Moreover, this interaction could be also stabilized with a hydrogen bond between the nitro group and the amine group of the imidazolidine ring of the molecule.[52]

To estimate the LOD of our system we fit the data using the following sigmoidal–logistic relation (red line in Fig. 4a):

$$\Delta\lambda_{shift} = \Delta\lambda_{max}/(1 + \exp(-k([I] - x_c))$$

where $\Delta\lambda_{max}$ represents the theoretical maximum shift, x_c the imidacloprid concentration corresponding to a shift of $\Delta\lambda_{max}/2$ and k a fit parameter. The experimental evaluation reported in Fig. 4 is well fitted using $\Delta\lambda_{max}$ = 36.6 ± 0.9 nm, k = 6.5 ± 0.3 mL ng^{-1} and x_c = 351 ± 13 ng mL^{-1}, with an $R^2 > 0.99$ and

a reduced $\chi^2 = 0.2$. Considering the intersection of the fit with the minimum detectable shift S_{LOD} of 3.3 nm of our system we estimate a LOD value for our nanosensor of 0.75 ng mL^{-1} (0.75 ppB). S_{LOD} was evaluated through the relation $S_{LOD} = K\sigma$ where $K = 3$ is a parameter relating to a confidence interval of 99% for a Gaussian distribution of the values and $\sigma = 1.1$ nm is the standard deviation of the signal achieved from the blank sample.[53] The standard deviation (SD) values estimated are reported as error bars in Fig. 4a, and the calculated percentage coefficients of variation (% CV = SD/mean × 100) indicate a good reproducibility of our measurements. Indeed, the % CVs, calculated for the tested concentrations above the LOD, range from 8 to 12%.

Non-specific adsorption tests were performed exploiting a metasurface functionalized with an anti-glyphosate polyclonal antibody using the CS_2 one-step method. This kind of reference sensor is unable to bind imidacloprid specifically and allows us to reveal non-specific imidacloprid adhesion onto the biofunctionalized metasurfaces. In this case, the LSPR shift registered upon 400 ng mL^{-1} imidacloprid incubation was 0.5 ± 0.6, proving the lack of imidacloprid non-specific adsorption onto the sensor surface.

Finally, the specificity of our biosensor for the detection of imidacloprid was evaluated using 2 different no-target insecticides (Fig. 4b). We tested a concentration of 400 ng mL^{-1} for glyphosate and fipronil, and we registered a % signal compared to the 400 ng mL^{-1} imidacloprid response of 17.5% and a 19.8%, respectively. We repeated the measurements after passivation of the biofunctionalized metasurface with 3% (w/w) BSA and in this case we revealed LSPR shifts lower than the S_{LOD} of our system for both pesticides. In particular, we achieved an 8.2% and a 11.3% response for glyphosate and fipronil, respectively, compared to the imidacloprid signal.

These results highlight how our system can represent an optimum tool for a sensitive and specific detection of the imidacloprid for concentrations ranging between 1 and 1000 ng mL^{-1}.

It must be mentioned that the obtained LOD value of 0.75 ppb is extremely competitive considering the imidacloprid detection systems reported in the literature.[13–18] Moreover, we believe that our work represents an outstanding result considering that is the first example of imidacloprid detection achieved using a LSPR tool.

In the future, we have planned to perform further experiments to improve the reproducibility, the detection time and to minimize the cross-reactivity of our immunosensor, also testing real samples.

4. Conclusions

In this work, we conceived a LSPR sensor made of a plasmonic 2D nanostructure based on a periodic arrangement of iso-Y gold NPs. Enhanced plasmonic properties of such a structure were analyzed through FEM simulations in detail. The nanopattern was fabricated using the EBL technique and morphologically characterized. We demonstrated that our sensor can be used for a very reliable, sensitive and specific detection of imidacloprid. Furthermore, to the best of our knowledge, it is the first time that a nano-patterned LSPR bio-sensor has been employed for imidacloprid detection. The plasmonic properties of the pattern were investigated experimentally and a bulk sensitivity of 412 nm RIU^{-1} was found. We functionalized the plasmonic surface using a smart one-step strategy never used so far for the direct antibody immobilization. A wide working concentration range between 1 and 1000 ng mL^{-1} and an extremely appealing LOD lower than 1 ng mL^{-1} were achieved. The specificity of the system was preliminarily tested using two other pesticides, achieving LSPR shifts lower than the S_{LOD} of our system. Our achievements show how the developed nanosensor is a valid alternative to traditional methods for pesticide detection that can be integrated with other devices to realize low-cost portable POC testing.

Author contributions

The manuscript was written through the contributions of all authors. These authors contributed equally. Conceptualization, L. P. and J. Z.; methodology, A. V. and M. R.; optical measurements, M. R.; investigation, A. V.; data analysis, M. R. and A. V.; writing – original draft preparation, L. P., M. R. and A. V.; writing – review and editing, V. M., D. S., M. R., A. V., and L. P.; supervision, L. P. All authors have read and agreed to the published version of the manuscript.

Conflicts of interest

There are no conflicts to declare.

Acknowledgements

The authors gratefully acknowledge support for this work from the Projects Program PNR 2015–2020 ''Proof of Concept'' funding the project ''H_2OSafety-Design and development of environmental sensors for the research of microbiological and chemical contaminants hazardous to health'' (POC01_00109).

References

1 T. Shivanandappa and Y. Rajashekar, Mode of action of plant-derived natural insecticides, *Advances in Plant Biopesticides*, Springer, India, 2014, pp. 323–345.
2 J. Kimura-Kuroda, Y. Komuta, Y. Kuroda, M. Hayashi and H. Kawano, Nicotine-like effects of the neonicotinoid insecticides acetamiprid and imidacloprid on cerebellar neurons from neonatal rats, *PLoS One*, 2012, **7**, e32432.
3 K. Matsuda, M. Shimomura, M. Ihara, M. Akamatsu and D. B. Sattelle, Neonicotinoids show selective and diverse actions on their nicotinic receptor targets: Electrophysiology, molecular biology, and receptor modeling studies, *Biosci., Biotechnol. Biochem.*, 2005, **69**, 1442–1452.

4 L. P. Sheets, Imidacloprid, in *Encyclopedia of Toxicology: Third Edition*, Elsevier, 2014, pp. 1000–1003, DOI: 10.1016/B978-0-12-386454-3.00153-6.
5 D. A. Thompson, *et al.*, A critical review on the potential impacts of neonicotinoid insecticide use: Current knowledge of environmental fate, toxicity, and implications for human health, *Environ. Sci.: Proces. Impacts*, 2020, **22**, 1315–1346.
6 W. Han, Y. Tian and X. Shen, Human exposure to neonicotinoid insecticides and the evaluation of their potential toxicity: An overview, *Chemosphere*, 2018, **192**, 59–65.
7 C. de Lima e Silva, *et al.*, Comparative toxicity of imidacloprid and thiacloprid to different species of soil invertebrates, *Ecotoxicology*, 2017, **26**, 555–564.
8 F. Sánchez-Bayo, K. Goka and D. Hayasaka, Contamination of the aquatic environment with neonicotinoids and its implication for ecosystems, *Front. Environ. Sci.*, 2016, **4**, 71.
9 M. Ihara and K. Matsuda, Neonicotinoids: Molecular mechanisms of action, insights into resistance and impact on pollinators, *Curr. Opin. Insect. Sci.*, 2018, **30**, 86–92.
10 R. J. Blake and L. G. Copping, Are neonicotinoids killing bees?, *Pest Manage. Sci.*, 2017, **73**, 1293–1294.
11 P. R. Whitehorn, S. O'Connor, F. L. Wackers and D. Goulson, Neonicotinoid pesticide reduces bumble bee colony growth and queen production, *Science*, 2012, **336**, 351–352.
12 E. C. Reynoso, E. Torres, F. Bettazzi and I. Palchetti, Trends and perspectives in immunosensors for determination of currently-used pesticides: The case of glyphosate, organophosphates, and neonicotinoids, *Biosensors*, 2019, **9**, 20.
13 K. L. Lee, *et al.*, Nanoplasmonic biochips for rapid label-free detection of imidacloprid pesticides with a smartphone, *Biosens. Bioelectron.*, 2016, **75**, 88–95.
14 S. H. Wang, *et al.*, Multichannel nanoplasmonic platform for imidacloprid and fipronil residues rapid screen detection, *Biosens. Bioelectron.*, 2020, **170**, 112677.
15 S. Zhao, J. Dong, H. J. Jeong, K. Okumura and H. Ueda, Rapid detection of the neonicotinoid insecticide imidacloprid using a quenchbody assay, *Anal. Bioanal. Chem.*, 2018, **410**, 4219–4226.
16 S. El-Akaad, *et al.*, Capacitive sensor based on molecularly imprinted polymers for detection of the insecticide imidacloprid in water, *Sci. Rep.*, 2020, **10**, 14479.
17 W. Zhang, *et al.*, A signal on-off ratiometric electrochemical sensor coupled with a molecular imprinted polymer for selective and stable determination of imidacloprid, *Biosens. Bioelectron.*, 2020, **154**, 112091.
18 S. Babazadeh, P. A. Moghaddam, S. Keshipour and K. Mollazade, Colorimetric sensing of imidacloprid in cucumber fruits using a graphene quantum dot/Au(III) chemosensor, *Sci. Rep.*, 2020, **10**, 14327.
19 O. R. Bolduc and J. F. Masson, Advances in surface plasmon resonance sensing with nanoparticles and thin films: Nanomaterials, surface chemistry, and hybrid plasmonic techniques, *Anal. Chem.*, 2011, **83**, 8057–8062.
20 J. L. Hammond, N. Bhalla, S. D. Rafiee and P. Estrela, Localized surface plasmon resonance as a biosensing platform for developing countries, *Biosensors*, 2014, **vol. 4**, 172–188.
21 S. Unser, I. Bruzas, J. He and L. Sagle, Localized surface plasmon resonance biosensing: Current challenges and approaches, *Sensors*, 2015, **15**, 15684–15716.
22 C. Genslein, *et al.*, Graphene-enhanced plasmonic nanohole arrays for environmental sensing in aqueous samples, *Beilstein J. Nanotechnol.*, 2016, **7**, 1564–1573.
23 D. A. Stuart, A. J. Haes, C. R. Yonzon, E. M. Hicks and R. P. Van Duyne, Biological applications of localised surface plasmonic phenomenae, *IEE Proc. Nanobiotechnol.*, 2005, **152**, 13–32.
24 A. J. Haes, S. Zou, G. C. Schatz and R. P. Van Duyne, Nanoscale optical biosensor: Short range distance dependence of the localized surface plasmon resonance of noble metal nanoparticles, *J. Phys. Chem. B*, 2004, **108**, 6961–6968.
25 A. J. Haes, S. Zou, G. C. Schatz and R. P. Van Duyne, A nanoscale optical biosensor: The long range distance dependence of the localized surface plasmon resonance of noble metal nanoparticles, *J. Phys. Chem. B*, 2004, **108**, 109–116.
26 J. Lin, Y. Zhang, J. Qian and S. He, A nano-plasmonic chip for simultaneous sensing with dual-resonance surface-enhanced Raman scattering and localized surface plasmon resonance, *Laser Photonics Rev.*, 2014, **8**, 610–616.
27 C. Huang, *et al.*, Localized surface plasmon resonance biosensor integrated with microfluidic chip, *Biomed. Microdevices*, 2009, **11**, 893–901.
28 S. Li, *et al.*, Electrophoresis-enhanced localized surface plasmon resonance sensing based on nanocup array for thrombin detection, *Sens. Actuators, B*, 2016, **232**, 219–225.
29 G. Qiu, S. P. Ng and L. C. M. Wu, Dielectric functionalization for differential phase detecting localized surface plasmon resonance biosensor, *Sens. Actuators, B*, 2016, **234**, 247–254.
30 X. Li, J. Zhu and B. Wei, Hybrid nanostructures of metal/two-dimensional nanomaterials for plasmon-enhanced applications, *Chem. Soc. Rev.*, 2016, **45**, 3145–3187.
31 M. Rippa, R. Castagna, V. Tkachenko, J. Zhou and L. Petti, Engineered nanopatterned substrates for high-sensitive localized surface plasmon resonance: An assay on biomacromolecules, *J. Mater. Chem. B*, 2017, **5**, 5473–5478.
32 Y. Ma, *et al.*, Localized surface plasmon resonance and surface enhanced Raman scattering responses of Au@Ag core–shell nanorods with different thickness of Ag shell, *J. Nanosci. Nanotechnol.*, 2014, **14**, 4245–4250.
33 D. Chen, J. Zhou, M. Rippa and L. Petti, Structure-dependent localized surface plasmon resonance characteristics and surface enhanced Raman scattering performances of quasi-periodic nanoarrays: Measurements and analysis, *J. Appl. Phys.*, 2015, **118**, 163101.
34 J. Jiang, *et al.*, Plasmonic nano-arrays for ultrasensitive biosensing, *Nanophotonics*, 2018, **7**, 1517–1531.
35 J. Cao, T. Sun and K. T. V. Grattan, Gold nanorod-based localized surface plasmon resonance biosensors: A review, *Sens. Actuators, B*, 2014, **195**, 332–351.
36 M. E. Stewart, *et al.*, Nanostructured plasmonic sensors, *Chem. Rev.*, 2008, **108**, 494–521.

37 F. Hao, C. L. Nehl, J. H. Hafner and P. Nordlander, Plasmon resonances of a gold nanostar, *Nano Lett.*, 2007, **7**, 729–732.
38 J. Sitjar, *et al.*, Ag nanostructures with spikes on adhesive tape as a flexible SERS-active substrate for *in situ* trace detection of pesticides on fruit skin, *Nanomaterials*, 2019, **9**, 1750.
39 O. Tokel, F. Inci and U. Demirci, Advances in plasmonic technologies for point of care applications, *Chem. Rev.*, 2014, **114**, 5728–5752.
40 G. Barbillon, *et al.*, Detection in near-field domain of biomolecules adsorbed on a single metallic nanoparticle, *J. Microsc.*, 2008, **229**, 270–274.
41 T. O. Paiva, *et al.*, Nanostructured interfaces with site-specific bioreceptors for immunosensing, *Appl. Surf. Sci.*, 2017, **412**, 455–463.
42 Y. Niu, A. I. Matos, L. M. Abrantes, A. S. Viana and G. Jin, Antibody oriented immobilization on gold using the reaction between carbon disulfide and amine groups and its application in immunosensing, *Langmuir*, 2012, **28**, 17718–17725.
43 J. Sharma, R. Chhabra, H. Yan and Y. Liu, A facile in situ generation of dithiocarbamate ligands for stable gold nanoparticle–oligonucleotide conjugates, *Chem. Commun.*, 2008, 2140–2142, DOI: 10.1039/b800109j.
44 I. Almeida, V. C. Ferreira, M. F. Montemor, L. M. Abrantes and A. S. Viana, One-pot approach to modify nanostructured gold surfaces through in situ dithiocarbamate linkages, *Electrochim. Acta*, 2012, **83**, 311–320.
45 I. Almeida, A. C. Cascalheira and A. S. Viana, One step gold (bio)functionalisation based on CS2-amine reaction, *Electrochim. Acta*, 2010, **55**, 8686–8695.
46 L. Zhao, Y. Jin, Z. Yan, Y. Liu and H. Zhu, Novel, highly selective detection of Cr(III) in aqueous solution based on a gold nanoparticles colorimetric assay and its application for determining Cr(VI), *Anal. Chim. Acta*, 2012, **731**, 75–81.
47 J. Homola, Surface plasmon resonance sensors for detection of chemical and biological species, *Chem. Rev.*, 2008, **108**, 462–493.
48 L. Pasquardini, *et al.*, A surface plasmon resonance plastic optical fiber biosensor for the detection of pancreatic amylase in surgically-placed drain effluent, *Sensors*, 2021, **21**, 3443.
49 B. Holzer, *et al.*, Characterization of covalently bound anti-human immunoglobulins on self-assembled monolayer modified gold electrodes, *Adv. Biosyst.*, 2017, **1**, 1700055.
50 S. C. Jena, *et al.*, Surface plasmon resonance immunosensor for label-free detection of BIRC5 biomarker in spontaneously occurring canine mammary tumours, *Sci. Rep.*, 2019, **9**, 13485.
51 L. Zhang, D. Hu, M. Salmain, B. Liedberg and S. Boujday, Direct quantification of surface coverage of antibody in IgG-Gold nanoparticles conjugates, *Talanta*, 2019, **204**, 875–881.
52 Y. Li, B. Qin, J. Zheng, Y. Gan and R. Yang, Intermolecular weak interaction of imidacloprid investigated by terahertz spectroscopy and theoretical calculation, *Optik*, 2021, **241**, 167063.
53 J. Homola and M. Piliarik, Surface plasmon resonance (SPR) sensors, *Springer Ser. Chem. Sens. Biosens.*, 2006, **4**, 45–67.